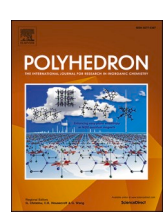
ELSEVIER

Contents lists available at ScienceDirect

Polyhedron

journal homepage: www.elsevier.com/locate/poly





Metallophilic interactions and magnetism in heterobimetallic {Pt,M} lantern complexes

Jesse L. Guillet ^a, Tarik J. Ozumerzifon ^b, Matthew P. Shores ^b, Curtis E. Moore ^c, Arnold L. Rheingold ^d, A. Timothy Royappa ^e, Linda H. Doerrer ^{f,*}

- ^a Environmental Resources Management, Boston, MA 02108, the United States of America
- b Department of Chemistry, Colorado State University, Fort Collins, CO 80523, the United States of America
- ^c Department of Chemistry, Ohio State University, Columbus, OH 43210, the United States of America
- ^d Department of Chemistry, University of California San Diego, La Jolla, CA 92093, the United States of America
- e Department of Chemistry, University of West Florida, Pensacola, FL 32514, the United States of America
- f Department of Chemistry, Boston University, Boston, MA 02215, the United States of America

ARTICLE INFO

Keywords: Lantern complexes Paddlewheel complexes Magnetic materials Heterobimetallic complexes Metallophilic interactions

ABSTRACT

A small series of polymeric heterobimetallic {Pt,M} lantern complexes of the form [PtM(SAc)₄DABCO]_∞ (SAc = thioacetate, DABCO = 1,4-diazabicyclo[2,2,2]octane; M = Co (1), Ni (2), Zn (3)) has been synthesized, along with the discrete molecular analog of each polymer formed by replacing DABCO with quinuclidine (4–6). All compounds except 3 have been structurally characterized by single-crystal X-ray diffraction. Compound 1 shows a metallophilic Pt Pt interaction of 3.1204(4) Å, while in 2 the same interaction is even shorter at 3.0944(10) Å. The electronic spectra of all compounds have been measured, which show d-d transitions of the 3d metal, Pt LMCT bands, and metal–metal charge transfer bands. Measurements of the temperature dependence of the magnetic susceptibility of 1 and 2 reveal antiferromagnetic exchange coupling between the 3d metal centers with J = -10 cm⁻¹ for Co-containing 1 and J = -32 cm⁻¹ between Ni centers for 2, both of which access the Pt Pt metallophilic interactions.

1. Introduction

The organization of homobimetallic lantern (paddlewheel) complexes into 1D systems has been the subject of much research effort, and DABCO (1,4-diazabicyclo[2,2,2]octane) has often been used for the formation of linear, quasi-1D chains due to its axial, bidentate binding character. In addition, much research has been done to probe the molecular orbital basis for magnetic coupling [1]. This ligand features two lone pairs separated by three σ bonds, as shown in Fig. 1 (right, bottom), as well as lone pairs that can interact through the empty σ^* orbitals running through the compound [2].

Magnetic exchange in a quasi-1D chain bridged by pyrazine (which also features two lone pairs separated by three σ bonds) was first reported in 1971 [3], in a chain composed of [Cu(NO₃)₂(pyz)]_∞ units that displayed an antiferromagnetic exchange of J=-6 cm⁻¹. Similarly, DABCO has been used to bridge {Mo₂} [4], {Cu₂} [5–9], {Cd₂} [6], {Zn₂} [6], and {Rh₂} [10] based lanterns into quasi-1D geometries, but no magnetic exchange across DABCO was observed. In addition to these

quasi-1D materials, DABCO has been used as a bridging ligand in metal organic frameworks (MOFs), linking $\{Co_2\}$ [11], $\{Ni_2\}$ [12], $\{Cu_2\}$ [13,14], and $\{Zn_2\}$ [11,13,15] based lantern units. For these MOFs no magnetic characterization has been reported to date.

The Doerrer group has developed a family of heterobimetallic lanterns of the form [PtM(SOCR)₄L], which feature Pt and a 3*d* metal linked by four thiocarboxylate (S(O=C)R, or SOCR for short) groups with homoleptic {PtS₄} and {MO₄} coordination [16–20]. We have previously reported compounds with M = Cr [19], Mn [19], Fe [16], Co [16–19], Ni [16–19], Zn [16–20], and the axially ligated L = H₂O [16,17,20], pyridine derivatives [17,18], NCS [19], and donating solvents (DMSO, DMF) [18]. Recently, we described [19] an example of a quasi-1D zig-zag chain of heterobimetallic lantern structures containing Cr³⁺ bridged by NCS in [PtCr(tba)₄(NCS)]_∞, but electrostatic barriers prevented the assembly of anionic [PtM^{II}(SOCR)₄(NCS)] units into extended arrays. The [PtM(SAc)₄(pyz)]_∞ (SAc = thioacetate) family of compounds (M = Co, Ni, Zn) has also been prepared [21]. In addition, an attempt to produce extended structures using Cl bridges by oxidation of

E-mail address: doerrer@bu.edu (L.H. Doerrer).

 $^{^{\}ast}$ Corresponding author.

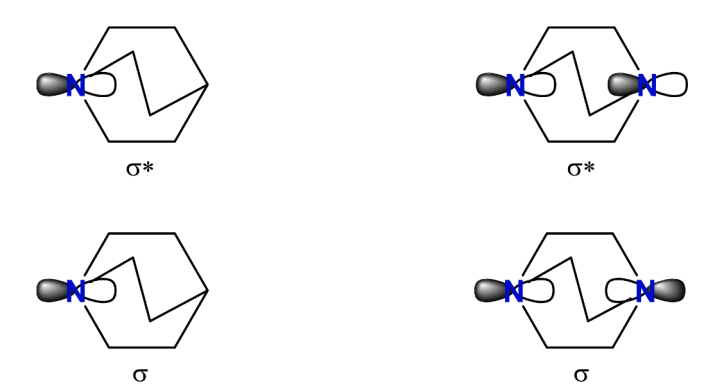


Fig. 1. Molecular orbitals on quinuclidine (left) and DABCO (right).

(PPN)[PtNi(tba) $_4$ Cl] was unsuccessful, and resulted in the discrete molecular species [ClPtNi(tba) $_4$ (OH $_2$)] [22], after an intramolecular ligand exchange of Cl 1 from Ni to Pt.

Beyond the heterobimetallic lanterns the Doerrer group has prepared, we have also recently reported a family of compounds based on the [Ni₂(SOCR)₄(L)] (R = CH₃, Ph) unit, with either bridging ligands (L = DABCO, pyz) or a terminal ligand (L = quinuclidine) [23]. The carboxylate ligands bind in a homoleptic fashion yielding a low-spin {NiS₄} center and a high-spin {NiO₄} center. In some homobimetallic lanterns with asymmetric ligands, cis-{MS₂O₂} coordination has been observed as in [Mo₂(tba)₄(OPPh₃)] [24]. The quasi-1D arrangements formed with DABCO and pyrazine show only very weak ($J = -0.1 \, \text{cm}^{-1}$) antiferromagnetic interactions between lantern units [23].

We have selected these heterobimetallic lantern complexes, [PtM (SOCR)₄(L)], with anisotropic structures potentially to engender the necessary properties for a single chain magnet (SCM). A related goal was to shed light on the extent to which metallophilic interactions affect the properties of such complexes in the solid state [25]. This system is a versatile scaffold that allows for the incorporation of various paramagnetic metal ions in the {MO₄} site and bridging (or terminal, for control studies) ligands and has in the past displayed strong interlantern magnetic interactions with limited inter-chain coupling detected. For example, several of the {PtM} lanterns that we have reported crystallize with a Pt...Pt metallophilic interaction, which facilitates strong anti-ferromagnetic coupling [16,17]. In the case of [PtM (tba)₄(OH₂)], the 3d metal atoms are antiferromagnetically coupled with $J = -60 \text{ cm}^{-1}$ for M = Ni and $J = -10 \text{ cm}^{-1}$ for M = Co [16]. Similar values of -50.8 (Ni) and -12.7 (Co) cm⁻¹ were observed in the $[PtM(SAc)_4(OH_2)]$ analogs, while weaker coupling constants of -12.6(Ni) and -6.0 (Co) cm⁻¹ were observed in [PtM(SAc)₄(pyNO₂)] [17]. The previously mentioned [PtCr(tba)₄(NCS)]_∞ displays an intrachain ferromagnetic interaction that supersedes the inter-chain interactions [19]. In the cases of [Ni₂(SOCR)₄(L)], mentioned above, there is only limited intra-chain coupling, while no inter-chain coupling was detected [23]. The use of lantern complexes in SCM design provides a new, facile method for organizing isolated spin centers into 1D arrays that are well isolated in the orthogonal directions.

Our broad goal has been to extend the range and variety of ligands on the 3d metals in such complexes, with a particular view to elucidating the magnetic interactions between two lanterns, especially the role of inter-dimer structural motifs and how they affect coupling (or the lack thereof) between the two 3d metals [26]. This project is part of our investigation into the properties of the building blocks in these quasi-1D systems, and how their magnetic properties are affected by metallophilic interactions inherent in the structure. Herein, we report the synthesis and characterization of two distinct groups of new lantern complexes. The first, $\{[PtM(SAc)_4]_2[DABCO]\}_{\infty}$, forms linear, quasi-1D chains, while the second, $[PtM(SAc)_4(quin)]$, (quin = quinuclidine), is the discrete molecular analog of the first. These compounds display distinct magnetic behavior, featuring antiferromagnetic exchanges across the

metallophilic {MPt}···{PtM} contact in the case of { $[PtM(SAc)_4]_2[-DABCO]$ }_∞ and isolated spin centers in the case of [$PtM(SAc)_4(quin)$].

2. Experimental methods

2.1. Starting materials and analytical methods

A series of literature procedures were used to prepare potassium tetrachloroplatinate (K_2PtCl_4) from platinum metal [27–29]. [PtM (SAc)₄(OH₂)] (M = Co, Ni, Zn) were prepared by published methods [17]. All other reagents were obtained commercially and used without further purification. UV-vis-NIR spectra were measured with a Shimadzu UV-3600 spectrometer. Diffuse reflectance UV-vis-NIR spectra were collected with a Harrick Praying Mantis attachment and were analyzed with the Kubelka-Munk transformation [30,31]. 1 H- and 13 C { 1 H}-NMR spectra were recorded on a Varian 500 MHz spectrometer and referenced to the residual protio solvent. Elemental analyses were performed by Atlantic Microlab Inc. (Norcross, GA).

2.2. Synthesis

{ [PtCo(SAc)₄] ₂(DABCO)} $_{\infty}$ (1). A portion of [PtCo(SAc)₄(OH₂)] (137.9 mg, 0.241 mmol) was dissolved in minimal acetone, yielding a purple solution. Separately, a solution of DABCO (14.1 mg, 0.121 mmol) in CH₂Cl₂ was prepared and chilled to 9 $^{\circ}$ C. A mixture of 50:50 acetone: CH₂Cl₂ was layered onto the DABCO solution, followed by the [PtCo (SAc)₄(OH₂)] solution. The mixture was stored at 9 $^{\circ}$ C while the two reactants diffused together. Dark purple fern-shaped crystals (110.0 mg, 74 % yield) suitable for X-ray analysis grow within two days. Anal. Calcd. for C₂₂H₃₆N₂O₈S₈Co₂Pt₂: C, 21.64 %; H, 2.97 %; N, 2.29 %. Found: C, 21.77 %; H, 2.94 %; N, 2.35 %. UV–vis-NIR (diffuse reflectance) (λ_{max} , nm (k/s)): 279 nm (37.2), 496 nm (1.0), 587 nm (0.4), 1244 nm (0.08).

{ [PtNi(SAc)_4] $_2$ (DABCO)} $_\infty$ (2). Compound 2 is prepared by a similar method to 1, by substituting [PtNi(SAc)_4(OH_2)] (137.9 mg, 0.241 mmol) for [PtCo(SAc)_4(OH_2)] in the reaction with DABCO (14.6 mg, 0.121 mml). Green fern-shaped crystals (71.2 mg, 44 % yield) suitable for X-ray analysis grow from the layered reactants within two days. Anal. Calcd. for $C_{22}H_{36}N_2O_8S_8Ni_2Pt_2$: C, 21.65 %; H, 2.97 %; N, 2.30 %. Found: C, 21.94 %; H, 2.85 %; N, 2.36 %. UV–vis-NIR (diffuse reflectance) (λ_{max} , nm (k/s)): 279 (81.8), 669 (1.0), 1236 (1.2).

{ [PtZn(SAc)₄] $_2$ (DABCO)} $_\infty$ (3). Compound 3 is prepared by a similar method to 1, by substituting [PtZn(SAc)₄(OH₂)] (138.0 mg, 0.241 mmol) for [PtCo(SAc)₄(OH₂)] in the reaction with DABCO (13.4 mg, 0.121 mmol). Yellow fern-shaped crystals (39.8 mg, 25 % yield) grow from the layered reactants within two days. Anal. Calcd. for $C_{22}H_{36}N_2O_8S_8Pt_2Zn_2$: C, 21.41 %; H, 2.94 %; N, 2.27 %. Found: C, 21.63 %; H, 2.85 %; N, 2.26 %. UV–vis-NIR (diffuse reflectance) (λ_{max} , nm (k/s)): 279 (1.0).

[PtCo(SAc)₄(quin)] (4). [PtCo(SAc)₄(OH₂)] (137.9 mg, 0.241 mmol) was dissolved in 10 mL acetone, yielding a purple solution. Quinuclidine (58.0 mg, 0.482 mmol) is dissolved in minimum acetone and added. The solution immediately turns to a dark magenta color and is stirred for 6 h. The solvent was removed on a Schlenk line and the remaining material was triturated with hexanes, yielding a bright magenta powder. Hexanes were used to wash the powder to a frit, and it was dried in vacuo overnight before massing (96.5 mg, 60 % yield). Magenta block-shaped crystals suitable for X-ray analysis were grown by layering a concentrated solution in diethyl ether with hexanes. Anal. calcd. for C₁₅H₂₅NO₄S₄CoPt: C, 27.11 %; H, 3.64 %; N 2.11 %. Found: C, 27.37 %; H, 3.70 %; N, 2.12 %. UV–vis-NIR (CH₂Cl₂) (λ_{max} , nm (ϵ_{M} , cm⁻¹ M⁻¹)): 253 (27,700), 508 (56.3), 529 (43.5), 1346 (5.3). μ_{eff} (Evans method, CH₂Cl₂): 4.43.

[PtNi(SAc)₄(quin)] (5). To obtain 5, [PtNi(SAc)₄(OH₂)] (137.9 mg, 0.241 mmol) was substituted for [PtCo(SAc)₄(OH₂)] in the preparation of 4 with quinuclidine (54.7 mg, 0.482 mmol), yielding a light green

powder (88.9 mg, 55 % yield). Green crystals suitable for X-ray analysis were grown by layering a concentrated solution in diethyl ether with hexanes. Anal. calcd. for $C_{15}H_{25}NO_4S_4NiPt$: C, 27.12 %; H, 3.64 %; N 2.11 %. Found: C, 27.30 %; H, 3.57 %; N, 2.21 %. UV–vis-NIR (CH₂Cl₂) (λ_{max} , nm (ϵ_{M} , cm⁻¹ M⁻¹)): 263 (46,400), 340 (3100), 699 (14.7), 1247 (10.4). μ_{eff} (Evans method, CH₂Cl₂): 3.01.

[PtZn(SAc)₄(quin)] (6). To obtain 6, [PtZn(SAc)₄(OH₂)] (138.0 mg, 0.241 mmol) was substituted for [PtCo(SAc)₄(OH₂)] in the preparation of 4 with quinuclidine (58.1 mg, 0.482 mmol), yielding a white powder (79.1 mg, 49 %). Colorless crystals suitable for X-ray analysis were grown by layering a concentrated solution in diethyl ether with hexanes. Anal. calcd. for C₁₅H₂₅NO₄S₄PtZn: C, 26.85 %; H, 3.61 %; N 2.09 %. Found: C, 26.98 %; H, 3.53 %; N, 2.10 %. UV–vis-NIR (CH₂Cl₂) (λ_{max} , nm (ε_M, cm⁻¹ M⁻¹)): 270 (21400). ¹H NMR, (δ, ppm, {CH₂Cl₂}): 3.25 (t, 3 J = 8.0 Hz, 6H, -N(CH₂CH₂)₃CH), 2.33 (s, 12H, SOCCH₃), 1.70 (td, 3 J = 8.0 Hz, 2.8 Hz, 6H, -N(CH₂CH₂)₃CH), 1.53 (broad s, 1H, -N (CH₂CH₂)₃CH). 13 C(1 H) NMR, (δ, ppm, {CH₂Cl₂}): 214.79 (s, SOCCH₃), 48.88 (s, -N(CH₂CH₂)₃CH), 33.15 (s, SOCCH₃), 26.08 (s, -N (CH₂CH₂)₃CH), 20.66 (s, -N(CH₂CH₂)₃CH).

2.3. Single crystal X-ray diffraction measurements

Suitable crystals were selected and data were collected on a Bruker APEX-II CCD diffractometer. The crystals were kept at 100 K during data collection. Using Olex2 [32], the structures were solved with the XT [33] structure solution program using direct methods and refined with the XL [34] refinement package using Least Squares minimization.

2.4. Magnetic measurements

Evans method [35,36] solution susceptibility measurements were performed for 4 and 5. $^1\mathrm{H}$ NMR spectra were collected on a Varian 500 MHz spectrometer. Solutions were prepared with $\mathrm{CD_2Cl_2}$ doped with hexamethyldisiloxane, and the change in chemical shift was measured for both the protio solvent and the $\mathrm{CH_3}$ protons of the hexamethyldisiloxane.

Magnetic susceptibility measurements for 1 and 2 were obtained using a Quantum Design MPMS-XL SQUID magnetometer. Measurements were made on solid crystalline samples sealed in a 1 cm \times 1.5 cm polyethylene bag and inserted into a clear plastic straw. Data were collected between 1.8 K and 300 K for dc applied fields ranging from -5 T to 5 T. The absence of ferromagnetic impurities was confirmed by the absence of deviations from linearity in the field scan of magnetization obtained at 100 K. The magnetic data were corrected for the magnetization of the sample holder by subtracting the signal from the sample holder and for diamagnetic contributions of the sample by using Pascal's

constants.

3. Results and discussion

3.1. Synthesis and structure

Compounds 1–6 were obtained from the previously reported [PtM (SAc)₄(OH₂)] lantern compounds, as shown in Scheme 1. Compounds 1, 2, and 4–6 have been crystallographically characterized and are discussed below.

Compounds 1-3 were made from freshly prepared [PtM (SAc)₄(OH₂)] and were crystallized directly from the reaction mixtures. Once formed, 1–3 are completely insoluble in common organic solvents, and therefore, in order to grow diffraction-quality crystals the reactants were allowed to mix as slowly as possible. The two solvents CH₂Cl₂ and acetone were chosen due to their favorable solubility (both reactants are soluble in each solvent) and because their differing densities allowed for the slow diffusion of the reactants. The reaction was monitored by checking the diffusion of the colored lantern layer (compared to the colorless DABCO layer). Crystals begin to form within one day, and the reactants have completely mixed within three. Due to the four-fold symmetry of the lantern unit compared to the three-fold symmetry of DABCO, there was quite a bit of crystallographic disorder in the DABCO ligand for all three compounds. In 1 and 2 this disorder was resolved, but in 3 only a connectivity model could be obtained from crystallographic analysis. The 2:1 lantern:bridge ratio, discussed below, was obtained even if the stoichiometry of the reactants was pushed to favor a 1:1 ratio, likely due to the very low solubility of the product. Future studies of the order of addition will attempt to saturate each Ni center with DABCO to prevent such bridging. In the structures of 1 and 2, the Platon SQUEEZE routine [37] was used to remove the diffraction contributions from disordered solvent molecules that could not be refined.

The monomeric unit of 1 obtained from its crystal structure is shown in Fig. 2 (top), and its quasi-1D chain structure is shown in Fig. 2 (bottom). The packing diagram of 1 is shown in Fig. 3. The structure contains only one unique lantern unit, with a Pt-Co distance of 2.6338 (6) Å. This distance is typical for this family of compounds, which have previously ranged only from 2.6223(9) Å (for L = DMSO) [18] to 2.669 (1) (for L = NCS) [19]. Two crystallographically related lantern units are bridged by a DABCO ligand in a ratio of two ligands to one lantern. Similarly, there is only one unique Co-N distance (2.158(3) Å) which is typical for a Co-N_{DABCO} distance, which averages 2.2(1) Å in 16 examples in the CSD [38–40]. This 2:1 unit is linked into a quasi-1D chain by a close metallophilic Pt⁻⁻⁻Pt interaction of 3.1204(4) Å. This distance is comparable to the analogous distance in [PtCo(SAc)₄(OH₂)] (3.1261(3) Å) [17] and is slightly longer than in [PtCo(tba)₄(OH₂)] (3.0650(3) Å)

Scheme 1. Synthesis of $\{[PtM(SAc)_4]_2(DABCO)\}_{\infty}$ (M = Co, 1; Ni, 2; Zn, 3) and $[PtM(SAc)_4(quin)]$ (M = Co, 4; Ni, 5; Zn, 6).

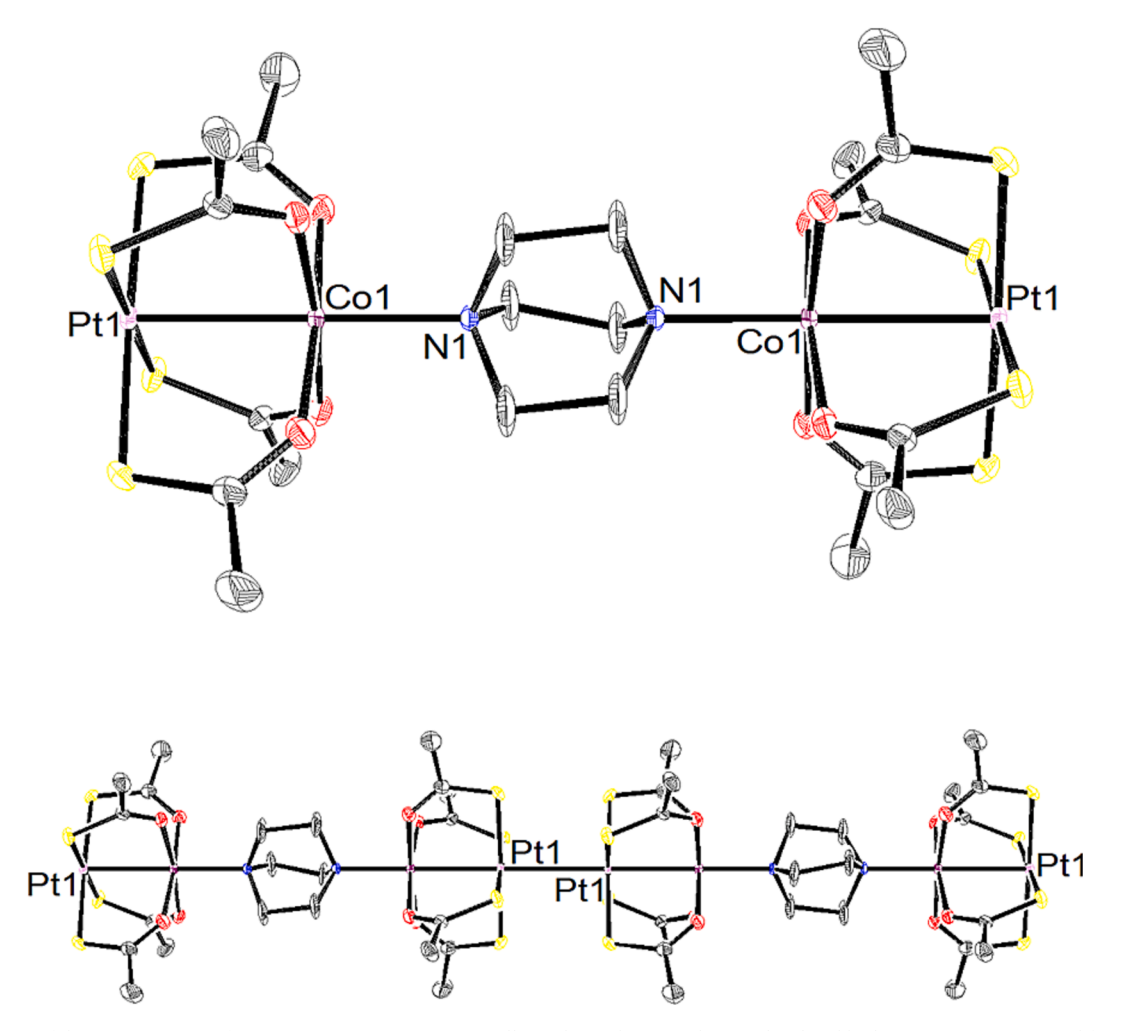


Fig. 2. (top) ORTEP of the repeating unit of $\{[PtCo(SAc)_4]_2(DABCO)\}_{\infty}$, 1. Ellipsoids are drawn at the 50% level and hydrogen atoms are omitted for clarity. The two lantern units shown are crystallographically identical. (bottom) Quasi-1D connection of $\{[PtCo(SAc)_4]_2(DABCO)\}_{\infty}$, 1, linked by a short Pt⁻⁻Pt metallophilic contact.

[16]. The interaction between these two {PtS₄} species is best categorized as a "staggered" geometry, from among the four different motifs seen to date [18,19]. This geometry is characterized by a short Pt⁻⁻Pt interaction and the eight thiocarboxylates being staggered from each other, rather than eclipsed [26]. The S-Pt-Pt-S torsion angle is 45.59(3)° and alternates within each repeating unit. These quasi-1D chains pack running alongside each other, as shown in Fig. 3, and which leads to three unique Co⁻⁻Co distances. The two shorter distances are both intrachain distances, with the shortest being 6.9141(7) Å across the DABCO ligand and the other being an 8.3880(7) Å distance across the Pt⁻⁻Pt interaction. The shortest inter-chain Co⁻⁻Co distance is 9.8480(3) Å.

Compound **2**, as shown in Fig. 4, is isostructural with **1**, and again has only one crystallographically unique lantern. The Pt-Ni distance (2.6054(15) Å) is, as expected, slightly shorter than the analogous Pt-Co distance, and the Ni-N distance is quite typical (2.073(9) Å). There are 22 examples in the CSD with a Ni-N_{DABCO} bond, which average a bond distance of 2.1(1) Å [38–40]. The Pt⁻⁻Pt interaction again links these 2:1 units into a quasi-1D chain, with a distance of 3.0944(10) Å, and like **1**, the interaction is best described by the staggered geometry [26], with a S-Pt-Pt-S torsion angle of 46.36(8)°. The chains again pack running alongside each other, leading to three unique Ni⁻⁻Ni distances, shown in Fig. 5. The three distances are 6.843(2) Å (across DABCO), 8.306(3) Å (across the Pt⁻⁻Pt interaction), and 9.835(3) Å (the shortest inter-chain distance).

Compounds **4–6** were prepared by a very similar method to what has been previously used to coordinate terminal ligands. The freshly prepared lantern complex is dissolved in acetone, and the reaction proceeds

immediately upon the addition of quinuclidine. Quinuclidine was chosen as a terminal analogue of DABCO. In the case of **4**, an obvious color change from light purple to a more intense magenta is seen immediately. No significant color change is visible for **5** (which maintains a green color) or **6** (colorless). In each case, some solid material may begin to precipitate immediately due to the lower solubility of the product. The powder that is recovered after removal of the reaction solvent is soluble in most organic solvents, though the solubility is quite low. Crystals are grown from diethyl ether/hexanes, and begin to grow overnight.

Compound 4 crystallizes as a monomer with only one crystallographically unique lantern ligated by a terminal quinuclidine ligand. Its intra-lantern bond distances are quite typical, with a Pt-Co distance of 2.6487(5) Å and a Co-N distance of 2.144(3) Å. The Pt-Co distance fits in the range of distances for this family of compounds, as discussed above. Quinuclidine has received relatively little use as a terminal capping ligand. There are only seven compounds that feature a late first-row transition metal coordinated to quinuclidine, which averaged a bond distance of 2.13(7) Å [38–40]. The crystal structure of 4 is shown in Fig. 6.

Compounds **5** and **6** have a similar structure to **4** and all three are isostructural with each other, with Pt-M distances of 2.6026(5) Å (for **5**) and 2.6815(5) Å (for **6**). The Pt-Ni distance for **5** is shorter than the Pt-Co distance for **4**, which is again consistent with previously reported compounds. Typically, the Pt-Zn distances are either the longest of the three (as is the case here) or between those of the Co and Ni analogues. The M-N distances are also consistent with **4**, with a Ni-N distance of 2.113(3) Å in **5** and a Zn-N distance of 2.096(2) Å in **6**. The distance in **5**

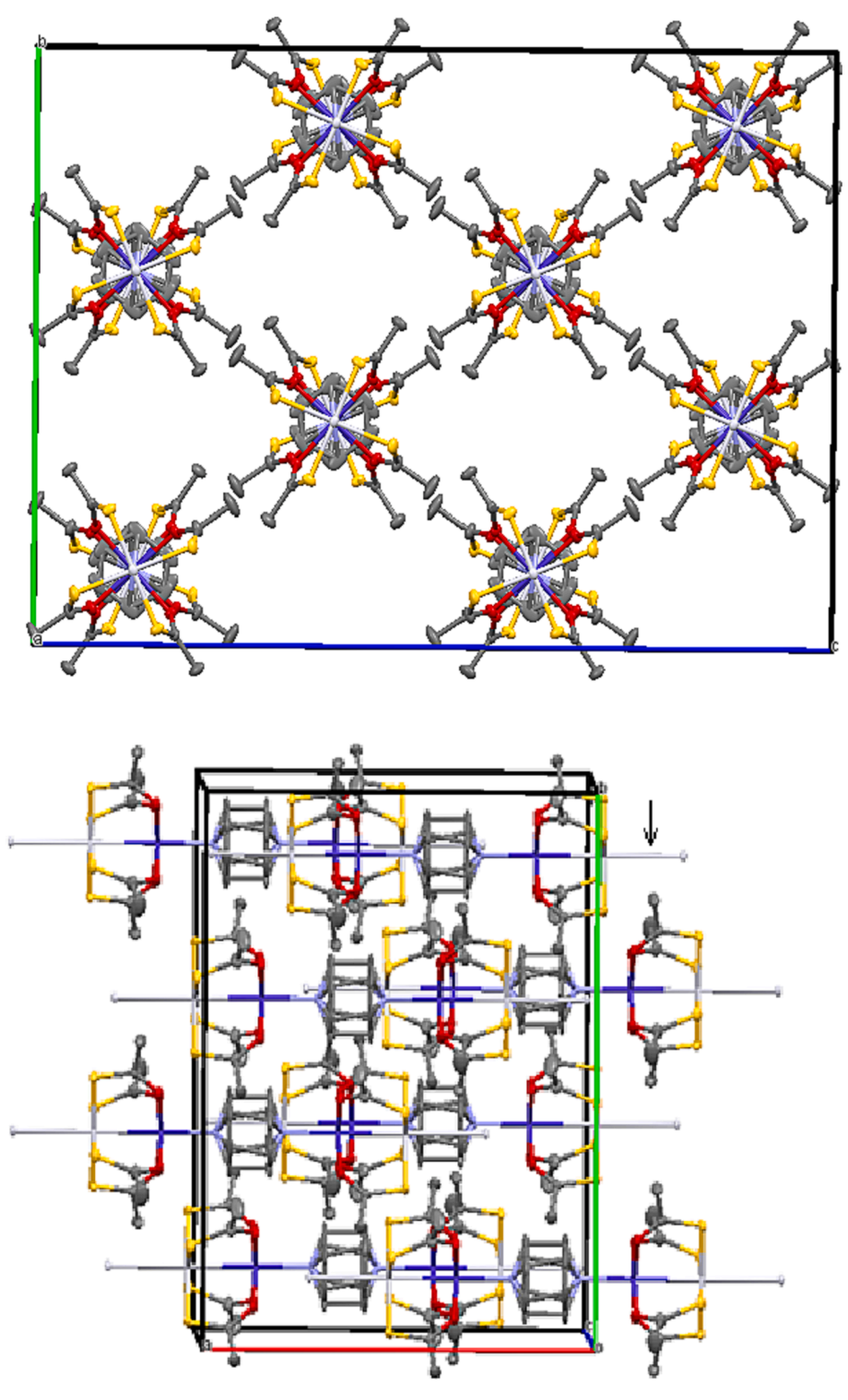


Fig. 3. (top) Packing diagram for {[PtCo(SAc)₄]₂(DABCO)}_{co}, 1, viewed down the Pt-M axis, showing the linear nature of the polymer chains. (bottom) View perpendicular to the Pt-M axis, with the metallophilic Pt⁻⁻Pt interaction indicated by the arrow at top right of picture.

is comparable to the Ni-N $_{quin}$ distance of 2.1238(16) Å in [Ni $_{2}$ (tba) $_{4}$ (-quin)] [23]. The structures for 5 and 6 are shown in Figs. 7 and 8 respectively.

This series represents a new model of inter-lantern interactions for this family of compounds. Previously [18,19], all compounds with a terminal ligand were split into four categories: (i) staggered, which was discussed above for 1; (ii) totally eclipsed, with a close Pt···Pt interaction and all ten atoms in the {PtS₄}-{PtS₄} pair aligned pair-wise; (iii) partially eclipsed, in which the Pt-S bonds are somewhat eclipsed but the

M-Pt-Pt angle is offset by about 160°; and (iv) square, in which the two Pt atoms and only two thiocarboxylate S atoms form a square [26]. In contrast, 4-6 have no close interactions between the Pt atom in one lantern and either a Pt atom or thiocarboxylate S atom from an adjacent lantern. The closest intermolecular contact to the Pt atom comes from the H atoms on an adjacent lantern's quinuclidine ligand. The closest contact is a Pt H contact, which measures 2.9756(2) Å for 4, 2.9644(3) Å for 5, and 2.9675(2) Å for 6. The packing diagram of 4, which is representative for the series, is shown in Fig. 9, which clearly shows the

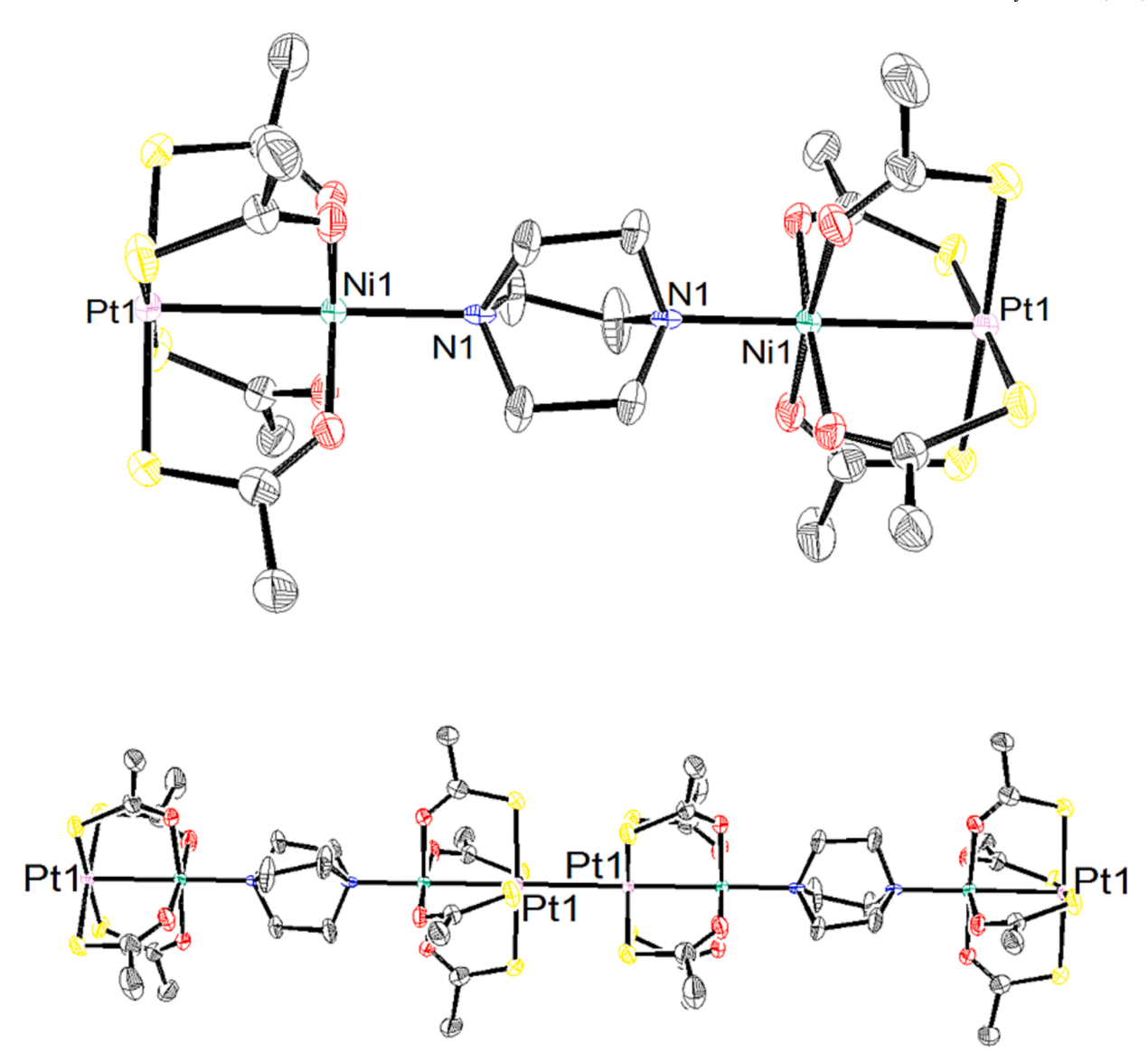


Fig. 4. (top) ORTEP of the repeating unit of $\{[PtNi(SAc)_4]_2(DABCO)\}_{\infty}$, 2. Ellipsoids are drawn at the 50% level and hydrogen atoms are omitted for clarity. The two lantern units shown are crystallographically identical. (bottom) Quasi-1D chain of $\{[PtNi(SAc)_4]_2(DABCO)\}_{\infty}$, 2, linked by a short metallophilic Pt⁻⁻Pt contact.

lack of Pt⁻⁻Pt contacts. The difference between the crystal packing of polymeric **1** and **2** and monomeric **4**, **5**, and **6** suggests that strength of the Pt⁻⁻Pt metallophilic interaction is similar in magnitude to the other weak crystal packing forces present in this family of compounds, which lack strong hydrogen bonding, π -stacking or ionic interactions. By changing the ratio of lantern-to-terminal-ligand, a net change in the intermolecular interactions appears.

X-ray crystallographic data collection parameters for single-crystal structures 1, 2, and 4–6 are listed in Table S1, and selected bond distances and angles in these structures are presented in Table S2. In general, the only noteworthy non-bonding interactions in all these crystal structures are the metallophilic interactions in 1–3; all others are standard van der Waals interactions.

3.2. Electronic structure and spectroscopy

Solution phase UV–vis spectra were collected for 4–6 and were as expected for compounds of this type based on previous data [16–19]. Compounds 4 and 5 display absorbances in the NIR at 1346 ($\epsilon_{M}=5.3~\text{M}^{-1}~\text{cm}^{-1}$) and 1247 ($\epsilon_{M}=10.4~\text{M}^{-1}~\text{cm}^{-1}$) nm, respectively, that are assigned as metal–metal charge transfers [16], as well as peaks in the

visible range that are assigned to *d-d* transitions centered on the 3d metal. For 4, these absorbances are observed at 508 ($\epsilon_{\rm M}=56.3~{\rm M}^{-1}~{\rm cm}^{-1}$) and 529 ($\epsilon_{\rm M}=43.5~{\rm M}^{-1}~{\rm cm}^{-1}$) nm, while for 5 the absorbance is at 699 ($\epsilon_{\rm M}=14.7~{\rm M}^{-1}~{\rm cm}^{-1}$) nm. These wavelengths, as well as the molar absorptivities, are consistent with previously reported {PtM} lantern structures [16–19]. As expected, these transitions are not observed for 6 due to the d^{10} electron configuration of Zn. All three of 4–6 display a strong absorbance in the UV that is assigned to a LMCT centered on the Pt atom [19,20]. These transitions are observed at 253 ($\epsilon_{\rm M}=27,700~{\rm M}^{-1}~{\rm cm}^{-1}$), 263 ($\epsilon_{\rm M}=46,400~{\rm M}^{-1}~{\rm cm}^{-1}$), and 270 ($\epsilon_{\rm M}=21,400~{\rm M}^{-1}~{\rm cm}^{-1}$) nm, respectively. The visible and NIR range of the spectra for 4 and 5 are shown in Fig. 10. The UV range of the spectra for 4–6 are shown in Fig. 11.

Due to the insolubility of 1–3, solid-state diffuse reflectance UV–vis spectra were collected, and the data were analyzed using the Kubelka-Munk transformation [30,31]. Similar to 4–6, which act as monomeric analogues, the observed transitions can be divided into three categories. First, 1 and 2 display transitions in the NIR (1, 1244 nm; 2, 1236 nm) and the visible range (1, 496 nm, 587 nm; 2, 669 nm) that are not seen in 3. In addition, each displays a strong transition in the UV range that is located at 279 nm for both 1 and 2, and is located 275 nm for 3. The

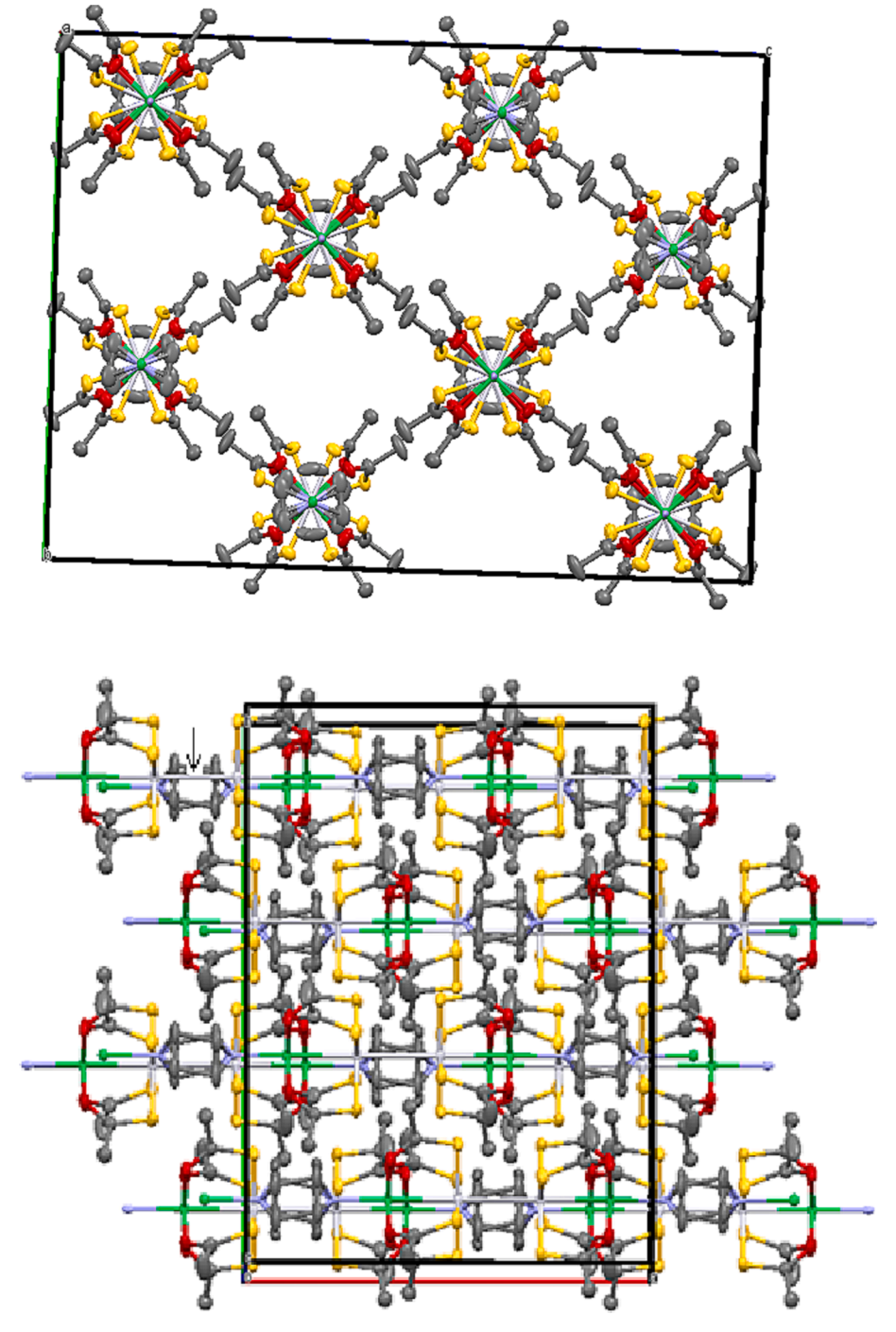


Fig. 5. Packing diagram for {[PtNi(SAc)₄]₂(DABCO)}_∞, 2, viewed (top) down the Pt-M axis and (bottom) parallel to the Pt-M axis.

spectra for 1 and 2 are shown in Figs. 12 and 13, respectively. Although there are close contacts that exist in the solid state when compared to the dilute solution environment for the spectra of 4–6, there are no significant changes displayed in the UV–vis-NIR spectra.

3.3. Magnetic measurements

Solution phase Evans method [35,36] measurements were collected for 4 and 5 and show μ_{eff} values of 4.43 and 3.01, respectively. These values are both higher than the predicted spin only magnetic moment (3.88 and 2.83) as has been true for others in this family of lantern compounds [18,19]. Previously, the Co analogues have ranged from $\mu_{eff}=4.61$ for L=py to 5.06 for $L=NO_2py$ [18]. The Ni analogues have

ranged from $\mu_{eff}=2.84$ for $L=OH_2$ [17] to 3.22 for $L=\underline{NCS}$ [19].

Solid state magnetic characterization was performed for **1** and **2**. The field dependence of magnetization was probed at 100 K and 200 K and was linear for both compounds, which is consistent with paramagnetic compounds and a lack of significant ferromagnetic impurities. The temperature dependence of magnetic susceptibility for **1** and **2** is shown in Fig. **14** and displays the paramagnetic nature of these compounds. The $\chi_M T$ value for **1** is 6.61 cm³ K mol⁻¹ at 300 K, and upon cooling a gradual decrease is observed until 135 K, where a discontinuity occurs and a steeper decrease occurs until 2 K, where $\chi_M T$ reaches 0.08 cm³ K mol⁻¹. Compound **2** follows a similar trend, as the room temperature $\chi_M T$ value is 2.28 cm³ K mol⁻¹, which decreases to a minimum of 0.02 cm³ K mol⁻¹ at 2 K. The discontinuity for each between 130 and 135 K is assigned to a

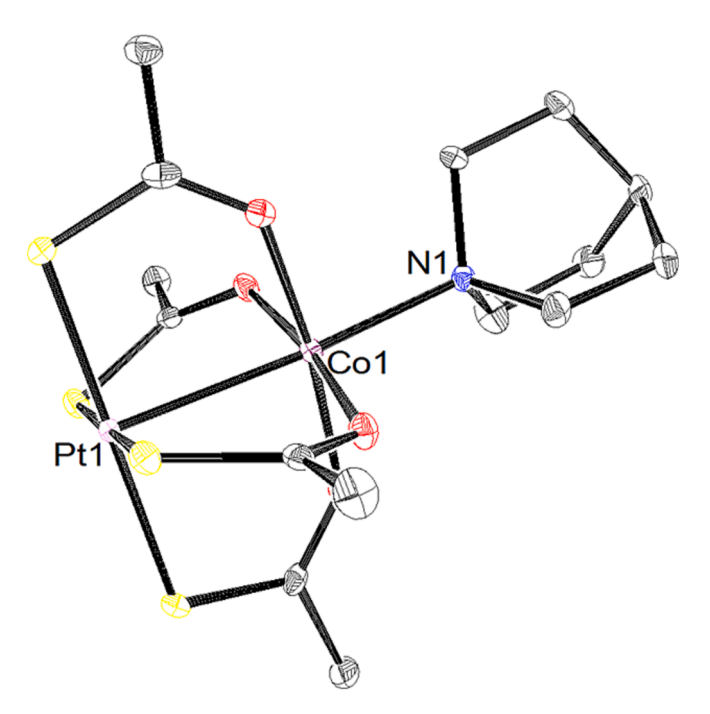


Fig. 6. ORTEP of the crystal structure of [PtCo(SAc)₄(quin)], **4.** Ellipsoids are drawn at the 50% level and hydrogen atoms are omitted for clarity.

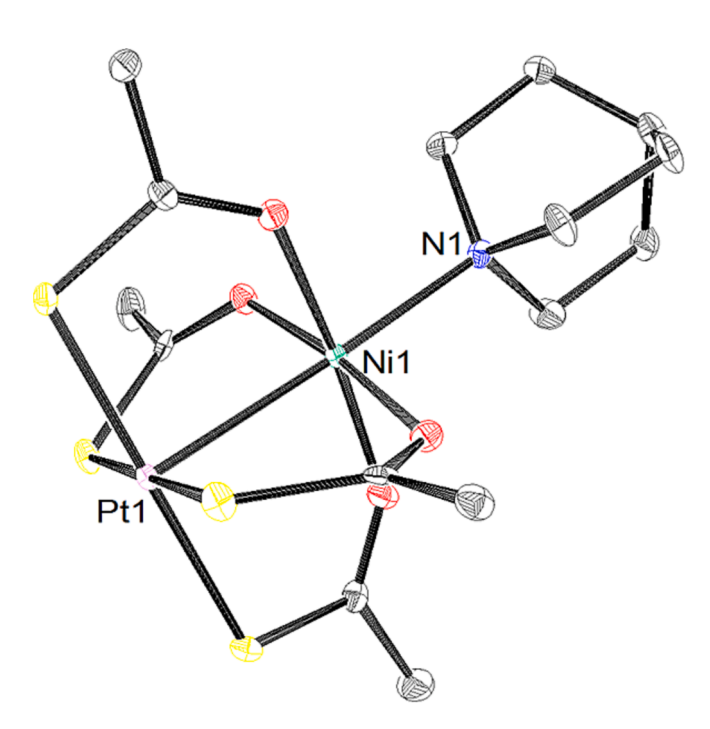


Fig. 7. ORTEP of [PtNi(SAc) $_4$ (quin)], 5. Ellipsoids are drawn at the 50% level and hydrogen atoms are omitted for clarity.

phase change, likely either a rotation of the lantern units with respect to each other or a rotation of the DABCO bridge. Again, significant crystallographic disorder was observed in the X-ray crystallographic data collected at 100 K.

These data are best fit when treated with a "dimer" model, as shown in Fig. 15, in which the magnetic exchange is across the Pt"Pt interaction with negligible interactions across the DABCO ligand and between chains, comparable to the modeling approach taken by others [41]. Fitting with the Hamiltonian:

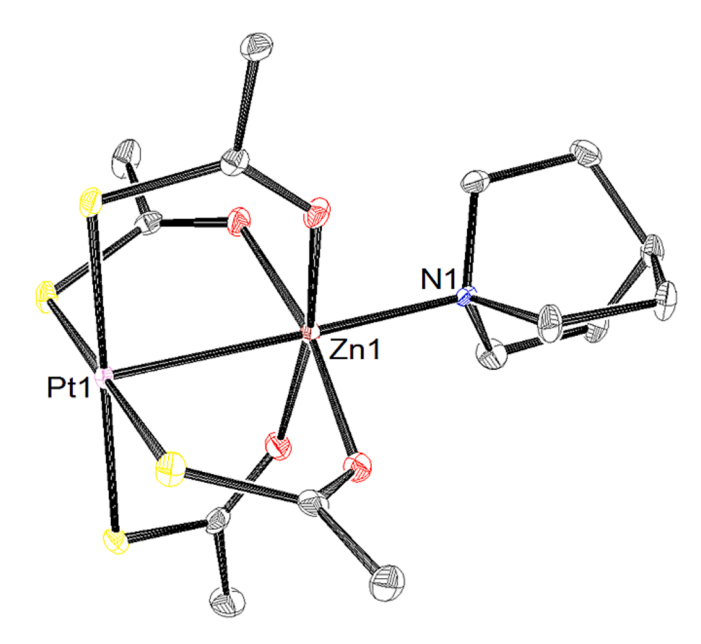


Fig. 8. ORTEP of [PtZn(SAc)₄(quin)], 6. Ellipsoids are drawn at the 50% level and hydrogen atoms are omitted for clarity.

$$\widehat{H} = -2J(S_A * S_B)$$

gives an antiferromagnetic exchange coupling of $J = -10 \text{ cm}^{-1}$ (for 1) or $J = -32 \text{ cm}^{-1}$ (for 2). This straightforward fit with a single coupling parameter *J* yielded good agreement with the data. Therefore, there was no need to construct a more elaborate chain model [42] involving two different, inseparable coupling parameters (J_{Pt-Pt} and J_{DABCO} for the two bridges), as it would have generated little insight. In any case, there is no obvious orbital pathway that communicates spin information between paramagnetic species bound to the DABCO nitrogens. The mostly-M SOMOs would then be orthogonal to each other, resulting in weak ferromagnetic coupling. The net effect of these competing interactions is likely that the "dimer" *J* is only slightly little less negative than might be expected if there were no DABCO bridge. We have previously demonstrated that this Pt...Pt interaction is capable of mediating antiferromagnetic interactions, where $J = -10 \text{ cm}^{-1}$ for [PtCo(tba)₄(OH₂)] and $-60 \text{ cm}^{-1} \text{ for } [PtNi(tba)_4(OH_2)] [16]; J = -12 \text{ cm}^{-1} \text{ for } [PtCo]$ $(SAc)_4(OH_2)$], $-50 \text{ cm}^{-1} \text{ for } [PtNi(SAc)_4(OH_2)]$, $-6 \text{ cm}^{-1} \text{ for } [PtCo]$ $(SAc)_4(pyNO_2)$], and -12 cm^{-1} for $[PtNi(SAc)_4(pyNO_2)]$ [17].

4. Conclusions

In summary, six new compounds have been prepared and their composition thoroughly characterized. These compounds include a new trio of quasi-1D chains, which have distinct structural motifs. Compounds 1–3 form chains composed of units of two lanterns and one bridging ligand linked into a quasi-1D architecture by close Pt^{...}Pt interactions of these {(lantern)₂(bridge)} trimers. Compounds 4–6 exist as discrete monomeric species, the first series in this family of {PtM} heterobimetallic lantern complexes without short Pt^{...}Pt or Pt^{...}L interactions.

In addition to their distinct structures, these six compounds show two distinct magnetic behaviors. Magnetic characterization of 1 and 2 revealed an antiferromagnetic exchange between 3d metal centers occurring primarily through the Pt⁻⁻Pt interaction, due to a more favorable electronic pathway despite the longer M–M distance between trimers than within. Solution-phase magnetic characterization by the Evans method shows that 4 and 5 act as isolated high spin metal centers, as is typical for the compounds of this family that do not form extended structures.

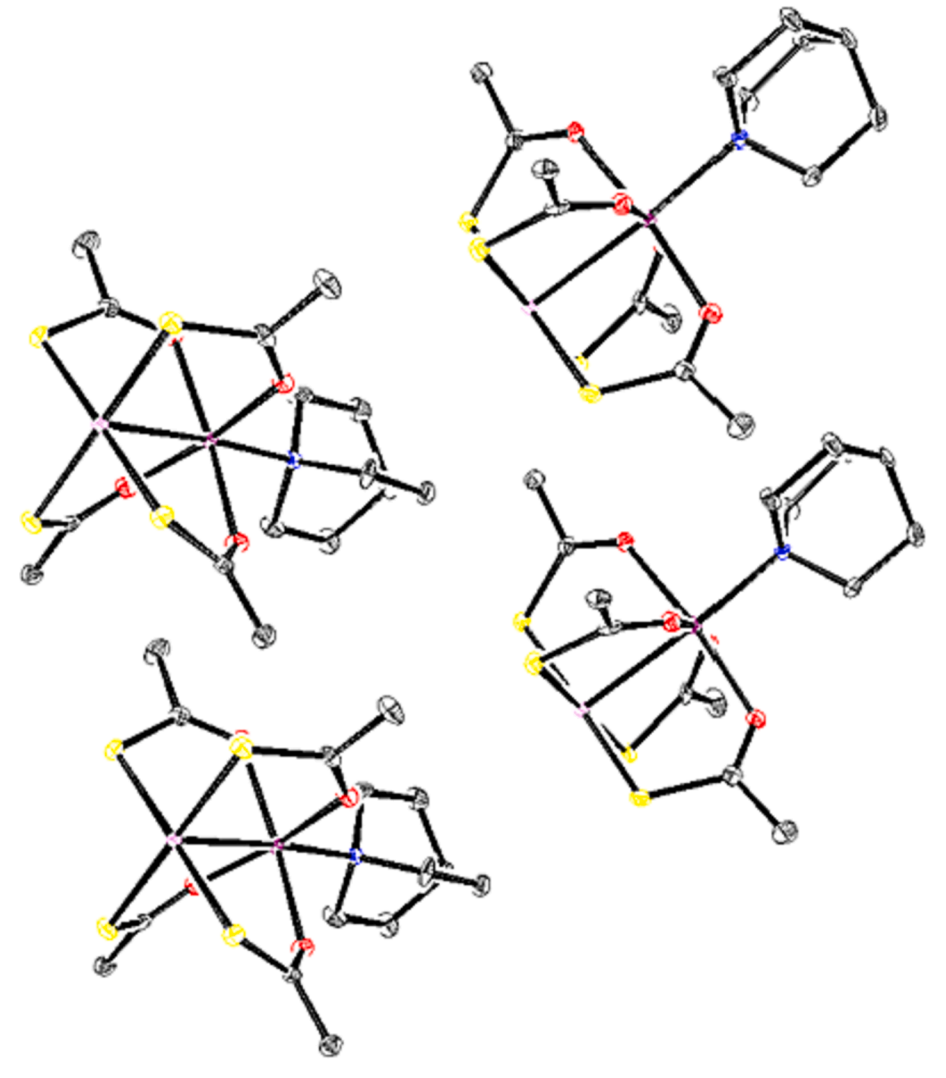


Fig. 9. Packing diagram for [PtCo(Sac)₄(quin)], 4, which is representative for 5 and 6 as well. Note the lack of a short Pt⁻⁻Pt or Pt⁻⁻S contact.

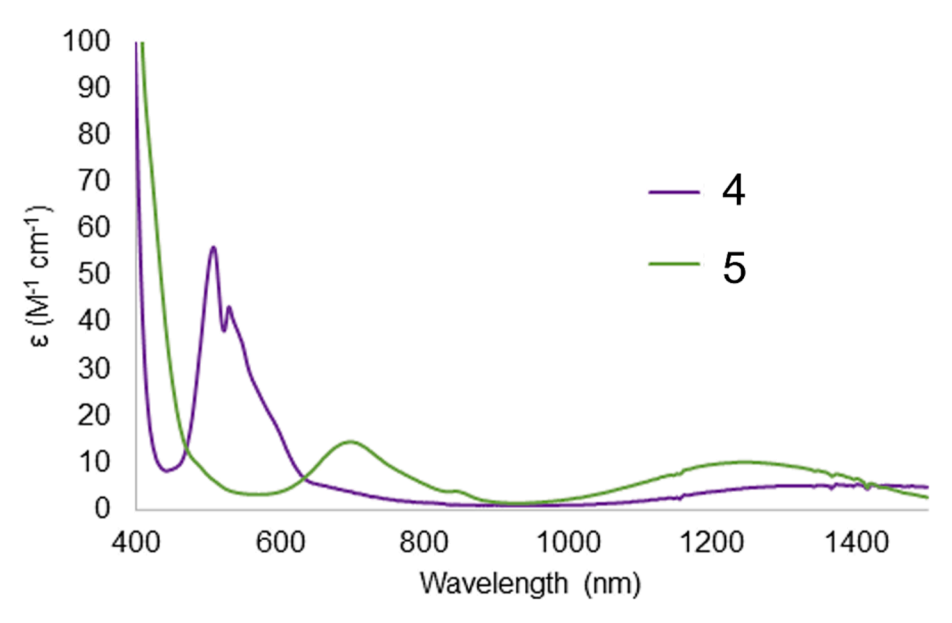
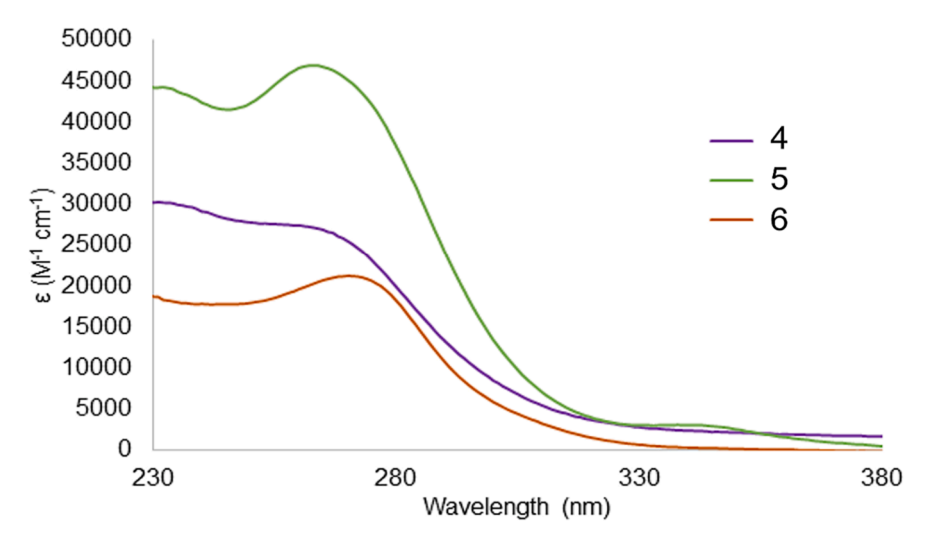


Fig. 10. Visible and NIR range of the electronic spectra for $[PtCo(SAc)_4(quin)]$, 4, and $[PtNi(SAc)_4(quin)]$, 5.



 $\label{eq:Fig. 11. UV range of the electronic spectra for [PtCo(SAc)_4(quin)], 4, [PtNi(SAc)_4(quin)], 5, and [PtZn(SAc)_4(quin)], 6. } \\$

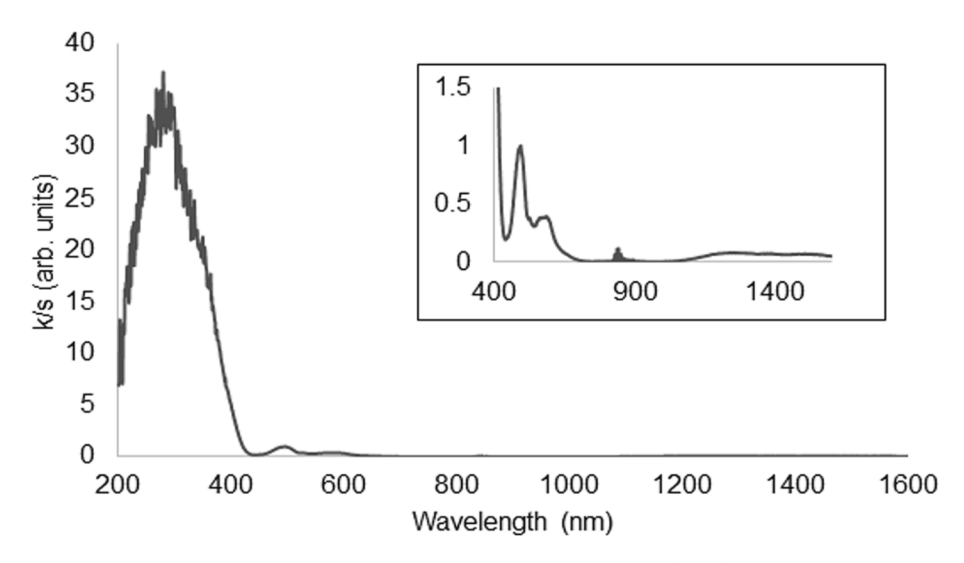


Fig. 12. Diffuse Reflectance UV–vis spectra for $\{[PtCo(SAc)_4]_2(DABCO)\}_{\infty}$, 1. The inset shows the visible and NIR ranges. The feature at ~ 850 nm is an artifact of the instrument.

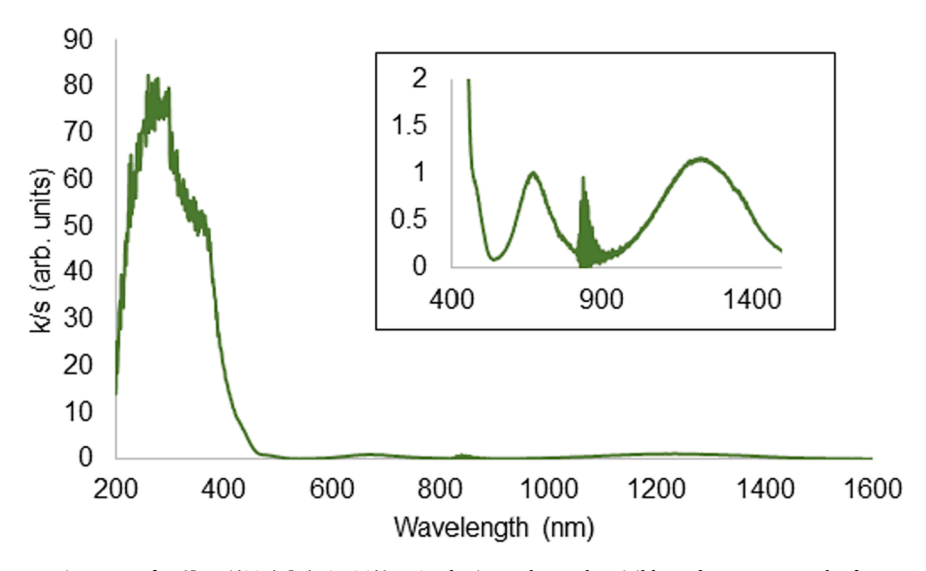


Fig. 13. Diffuse Reflectance UV–vis spectra for $\{[PtNi(SAc)_4]_2(DABCO)\}_{\infty}$, 2. The inset shows the visible and NIR ranges. The feature at \sim 850 nm is an artifact of the instrument.

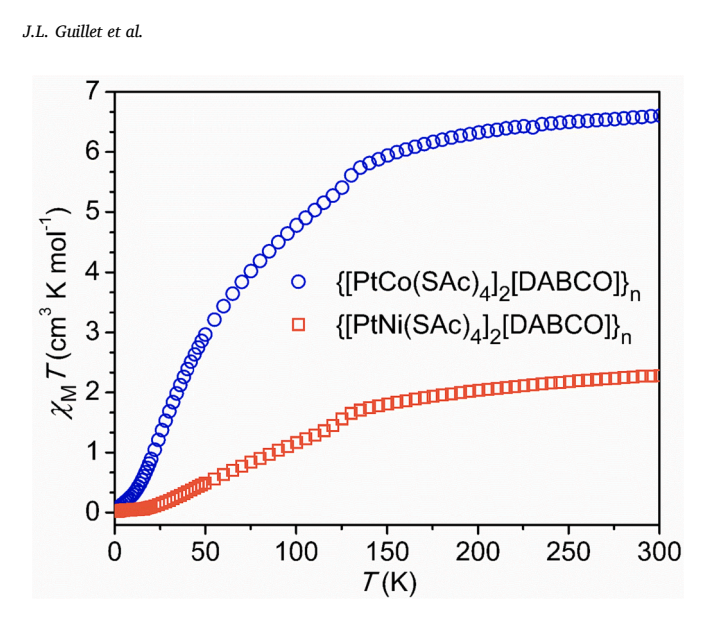


Fig. 14. Temperature dependence of magnetic susceptibility for {[PtM $(SAC)_4]_2[DABCO]}_{\infty}$ (M = Co, 1; Ni, 2), collected at an applied field of 1000 Oe.

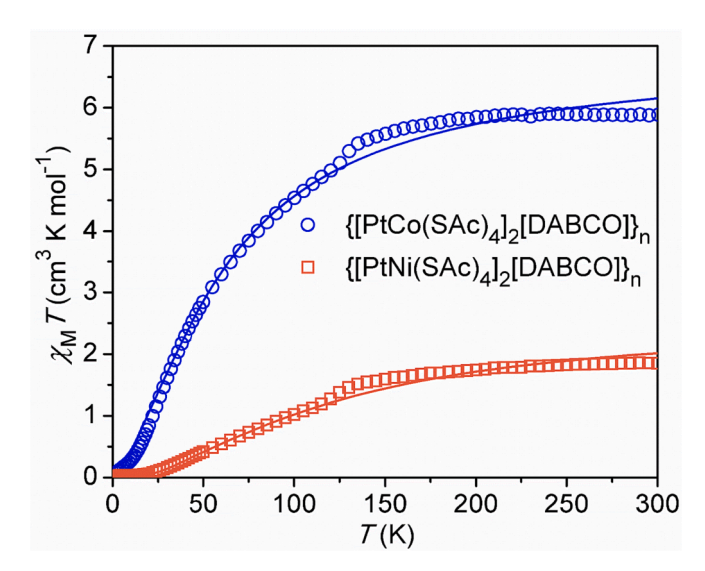


Fig. 15. Temperature dependence of magnetic susceptibilities for {[PtM $(SAc)_4]_2[DABCO]$ } $_\infty$ (M = Co, 1; Ni, 2) collected at an applied field of 1000 Oe. Temperature independent paramagnetism (TIP) has been subtracted from the data shown. Lines indicate current best fits to the data using a dimer model.

CRediT authorship contribution statement

Jesse L. Guillet: Investigation, Writing – original draft. Tarik J. Ozumerzifon: Formal analysis, Investigation. Matthew P. Shores: Formal analysis, Writing – original draft. Curtis E. Moore: Formal analysis, Investigation. Arnold L. Rheingold: Formal analysis, Investigation. A. Timothy Royappa: Formal analysis, Investigation, Writing – review & editing. Linda H. Doerrer: .

Declaration of competing interest

The authors declare that they have no known competing financial interests or personal relationships that could have appeared to influence the work reported in this paper.

Data availability

Data will be made available on request.

Acknowledgments

This project was supported by National Science Foundation grants NSF-NMR 0619339 (to Boston University) and NSF-CHE 1363274 and 1956399 (to M.P.S.).

Appendix A. Supplementary data

Supplementary data to this article can be found online at $\frac{\text{https:}}{\text{doi.}}$ org/10.1016/j.poly.2023.116788.

References

- [1] P.J. Hay, J.C. Thibeault, R. Hoffmann, J. Am. Chem. Soc. 97 (1975) 4884.
- [2] M.S. Haddad, D.N. Hendrickson, J.P. Cannady, R.S. Drago, D.S. Bieksza, J. Am. Chem. Soc. 101 (1979) 898.
- [3] W.E. Hatfield, J.F. Villa, J. Am. Chem. Soc. 93 (1971) 4081.
- [4] M. Handa, M. Mikuriya, T. Kotera, K. Yamada, T. Nakao, H. Matsumoto, K. Kasuga, Bull. Chem. Soc. Jpn. 68 (1995) 2567.
- [5] V.M. Rao, D.N. Sathyanarayana, H.J. Manohar, Chem, Dalton Trans, Soc., 1983,
- [6] R. Saravanakumar, B. Varghese, S. Sankararaman, J. Mol. Struct. 1076 (2014) 280.
- [7] C.-S. Liu, J.-J. Wang, L.-F. Yan, Z. Chang, X.-H. Bu, E.C. Sañudo, J. Ribas, Inorg. Chem. 46 (2007) 6299.
- [8] Y.L. Zhou, H.Y. He, L.G.Z. Zhu, Kristallogr. New Cryst. Struct. 220 (2005) 381.
- [9] A.D. Burrows, M.F. Mahon, P.R. Raithby, A.J. Warren, S.J. Teat, J.E. Warren, CrystEngComm 14 (2012) 3658.
- [10] M. Mikuriya, J. Yamamoto, K. Ouchi, D. Yoshioka, H. Tanaka, M. Handa, X-Ray Struct. Anal, Online 29 (2013) 45.
- [11] H. Chun, H. Jung, J. Seo, Inorg. Chem. 48 (2009) 2043.
- [12] V. Bon, N. Klein, I. Senkovska, A. Heerwig, J. Getzschmann, D. Wallacher, I. Zizak, M. Brzhezinskaya, U. Mueller, S. Kaskel, PCCP 17 (2015) 17471.
- [13] S. Furukawa, K. Hirai, K. Nakagawa, Y. Takashima, R. Matsuda, T. Tsuruoka, M. Kondo, R. Haruki, D. Tanaka, H. Sakamoto, S. Shimomura, O. Sakata, S. Kitagawa, Angew. Chem. Int. Ed. 48 (2009) 1766.
- [14] P. Müller, F.M. Wisser, V. Bon, R. Grünker, I. Senkovska, S. Kaskel, Chem. Mater. 27 (2015) 2460.
- [15] D.N. Dybtsev, H. Chun, K. Kim, Angew. Chem. Int. Ed. 43 (2004) 5033.
- [16] E.W. Dahl, F.G. Baddour, S.R. Fiedler, W.A. Hoffert, M.P. Shores, G.T. Yee, J.-P. Djukic, J.W. Bacon, A.L. Rheingold, L.H. Doerrer, Chem. Sci. 3 (2012) 602.
- [17] F.G. Baddour, S.R. Fiedler, M.P. Shores, J.A. Golen, A.L. Rheingold, L.H. Doerrer, Inorg. Chem. 52 (2013) 4926.
- [18] F.G. Baddour, S.R. Fiedler, M.P. Shores, J.W. Bacon, J.A. Golen, A.L. Rheingold, L. H. Doerrer, Inorg. Chem. 52 (2013) 13562.
- [19] J.L. Guillet, I. Bhowmick, M.P. Shores, C.J.A. Daley, M. Gembicky, J.A. Golen, A. L. Rheingold, L.H. Doerrer, Inorg. Chem. 55 (2016) 8099.
- [20] F.G. Baddour, A.S. Hyre, J.L. Guillet, D. Pascual, J.M. Lopez-de-Luzuriaga, T. M. Alam, J.W. Bacon, L.H. Doerrer, Inorg. Chem. 56 (2017) 452.
- [21] Baddour, F. G., Boston University, 2013.
- [22] M. Gennari, G. Givaja, O. Castillo, L. Hermosilla, C.J. Gómez-García, C. Duboc, A. Lledós, R. Mas-Ballesté, F. Zamora, Inorg. Chem. 53 (2014) 10553.
- [23] A. Nimthong-Roldan, J.L. Guillet, J. McNeely, T.J. Ozumerzifon, M.P. Shores, J. A. Golen, A.L. Rheingold, L.H. Doerrer, Dalton Trans. 46 (2017) 5546.
- [24] M. Cindric, V. Vrdoljak, D. Matkovic-Calogovic, B. Kamenar, Acta Crystallographica Section C 52 (1996) 3016.
- [25] Doerrer, L. H.; Del Rosario, C.; Fan, A. Metallophilic Interactions. In Comprehensive Inorganic Chemistry III (3rd ed.); Reedijk, J., Poeppelmeier, K. R., Eds.; Elsevier, 2023; Vol. 3, pp 665-739.
- [26] S.A. Beach, L.H. Doerrer, Acc. Chem Res. 51 (2018) 1063.
- [27] Kauffman, G. B.; Cowan, D. O. Inorg. Syn. (Jacob Kleinberg, editor. McGraw) 1963, 7, 239.
- [28] G.B. Kauffman, Inorg. Synth. 9 (1967) 182.
- [29] R.N. Keller, Inorg. Syntheses II (1946) 247.
- [30] P. Kubelka, F.Z. Munk, Tech. Physik 12 (1931) 593.
- [31] M.P. Diebold, Application of Light Scattering to Coatings: A User's Guide, Springer, 2014.
- [32] O.V. Dolomanov, L.J. Bourhis, R.J. Gildea, J.A.K. Howard, H. Puschmann, J. Appl. Crystallogr. 42 (2009) 339.
- [33] G.M. Sheldrick, Acta Crystallogr., Sect. A: Found. Adv. 71 (2015) 3.
- [34] G.M. Sheldrick, Acta Crystallogr. Sect. A 64 (2008) 112.
- [35] D.F. Evans, J. Chem. Soc. (1959, 2003.).
- [36] S.K. Sur, J. Magn. Reson. 82 (1989) 169.
- [37] A.L. Spek, Acta Crystallogr. Sect. C, Struct. Chem. C71 (2015) 9.
- [38] F.H. Allen, Acta Crystallogr. Sect. b: Struct. Sci. 58 (2002) 380.
- [39] F.H. Allen, W.D.S. Motherwell, Acta Crystallogr., Sect. b: Struct. Sci. B58 (2002) 407.
- [40] J.W. Yao, J.C. Cole, E. Pidcock, F.H. Allen, J.A.K. Howard, W.D.S. Motherwell, Acta Crystallogr., Sect. b: Struct. Sci. B58 (2002) 640.
- [41] A. Takamori, K. Uemura, Inorg. Chem. 61 (2022) 5762.
- [42] K. Uemura, A. Takamori, Coord. Chem. Rev. 471 (2022), 214736.